

Muon Spin Relaxation Study of Spin Dynamics in Quantum Spin Liquid Candidate $\text{H}_3\text{LiIr}_2\text{O}_6$

Yan-Xing Yang,^{1,*} Liang-Long Huang,^{2,*} Zi-Hao Zhu,¹ Chang-Sheng Chen,¹ Qiong Wu,¹
Zhao-Feng Ding,¹ Cheng Tan,¹ Pabi K. Biswas,³ Adrian D. Hillier,³ You-Guo Shi,^{4,5}
Da-Peng Yu,^{2,6} Cai Liu,^{2,6} Le Wang,^{2,6} Fei Ye,^{2,6} Jia-Wei Mei,^{2,6,†} and Lei Shu^{1,7,‡}

¹State Key Laboratory of Surface Physics, Department of Physics, Fudan University, Shanghai 200438, China

²Shenzhen Institute for Quantum Science and Engineering, and Department of Physics,
Southern University of Science and Technology, Shenzhen 518055, China

³ISIS Facility, STFC Rutherford Appleton Laboratory, Chilton, Didcot, Oxfordshire, OX110QX, United Kingdom

⁴Institute of Physics, Chinese Academy of Sciences, Beijing 100190, China

⁵School of Physical Sciences, University of Chinese Academy of Sciences, Beijing 100190, China

⁶Shenzhen Key Laboratory of Quantum Science and Engineering, Shenzhen 518055, PR China.

⁷Shanghai Research Center for Quantum Sciences, Shanghai 201315, China

(Dated: February 1, 2022)

We present detail thermodynamic and muon spin relaxation (μSR) studies of quantum spin liquid (QSL) candidate $\text{H}_3\text{LiIr}_2\text{O}_6$. In agreement with the low temperature thermodynamic evidence (*e.g.* bulk magnetization and heat capacity) for the absence of magnetic transition, zero-field (ZF)- μSR measurements indicate the absence of static magnetic ordering or spin freezing down to our lowest temperature of 80 mK. Both ZF- and longitudinal-field (LF)- μSR measurements reveal persistent spin fluctuations at low temperatures. These results provide well-established evidence of a QSL state in $\text{H}_3\text{LiIr}_2\text{O}_6$. Furthermore, the observation of the time-field scaling behavior of μSR spectra $A(t) \sim A(t/H^{0.46})$, and the low temperature power-law specific heat coefficient $C/T \sim T^{-0.57}$, indicate the finite density of state in the form of $N(E) \sim E^{-0.5}$, in a good agreement with the disorder-induced states in the Kitaev spin liquid.

Introduction. – Quantum spin liquid (QSL) is a highly entangled quantum state in the spin system where the spin degree of freedom does not freeze even at zero temperature, but highly entangles with each other [1–8]. The delicate many-body entanglement in QSL is a crucial ingredient for the mechanism of high-temperature superconductivity [2] and the implementation of topological quantum computation [9]. The exact solvable Kitaev honeycomb spin model [3] establishes the very existence of QSL in a simple spin interacting system, and the materialization of the Kitaev QSL in the experiments has been initialized currently [10–12]. With the help of the intertwining among magnetism, spin-orbital coupling, and crystal field, Ir^{4+} oxides and a Ru^{3+} chloride with a d^5 electronic configuration are promising to materialize the Kitaev model [13–16]. However, due to the non-Kitaev terms, these Kitaev compounds (*e.g.* $\alpha\text{-Li}_2\text{IrO}_3$ and $\alpha\text{-RuCl}_3$) usually develops long-range magnetic orders at low temperatures [13, 17, 18]. Although there are several experimental signatures of fractionalized high-energy spin excitations [19–21], magnetic orders preclude the access to the low-energy and low-temperature properties of QSL.

Chemical modification of $\alpha\text{-Li}_2\text{IrO}_3$ leads to the second generation of two-dimensional honeycomb iridates $\text{H}_3\text{LiIr}_2\text{O}_6$ [22–24]. Thermodynamic and NMR measurements did not detect any magnetic order transition down to low temperatures, establishing a possible QSL ground state in $\text{H}_3\text{LiIr}_2\text{O}_6$ [23]. Magnetic Raman spectroscopic study on single-crystal $\text{H}_3\text{LiIr}_2\text{O}_6$ samples reveals a dome-shaped magnetic Raman continuum [24], related to the high-energy fractionalized spin excitations ($\gtrsim 2$ meV) [25]. The non-magnetic disorder in $\text{H}_3\text{LiIr}_2\text{O}_6$ has various forms of stacking faults [22–24], the randomness of intercalated H posi-

tions [24, 26], and non-magnetic Ir^{3+} defects with a lower-oxidation-state configuration $3d^6$ [24]. The disorder suppresses the long-range magnetic order and releases the QSL properties covered by the magnetic order, leading to new phenomena as a cooperative manifestation of disordered topological condensed matter systems [27–34]. The non-magnetic disorder may nucleate exotic excitations, providing additional information on QSL. In $\text{H}_3\text{LiIr}_2\text{O}_6$, at odds with the thermodynamics of the pure Kitaev QSL, the abundant low-energy density of states (DOS) are observed in the heat capacity where the specific heat coefficient displays a low-temperature (less than 1 K) divergence of $C/T \sim T^{-0.5}$ [23], related to the disorder-induced states in the Kitaev QSL [23, 33, 34].

This letter reports detailed muon spin relaxation studies of the spin dynamics in $\text{H}_3\text{LiIr}_2\text{O}_6$ to reveal the disorder-induced finite DOS. Consistent with previous studies [23], our magnetization and heat capacity measurements do not detect any magnetic order transition in $\text{H}_3\text{LiIr}_2\text{O}_6$. The zero-field (ZF)- μSR shows no sign of static magnetic ordering, and both ZF- and longitudinal field (LF)- μSR measurements indicate persistent spin fluctuations down to our lowest temperature of 80 mK. To establish the relationship between the low-energy spin fluctuations and the disorder-induced DOS, magnetic field dependence of spin dynamics is studied and the time-field scaling behavior of μSR asymmetry spectra, $A(t) \sim A(t/H^\alpha)$ ($\alpha = 0.46$), is revealed at low applied magnetic fields. This implies the scaling of local spin dynamics $q(t) = \langle S_i(t)S_i(0) \rangle \sim t^{\alpha-1} \exp(-\lambda t)$. We stress that the critical exponent $\alpha = 0.46$ is related to the disorder-induced low-energy DOS of the form $N(E) \sim E^{-0.5}$ [23, 33, 34], with the same origin as our measured specific heat low-temperature divergence of $C/T \sim T^{-0.57}$. Our μSR studies

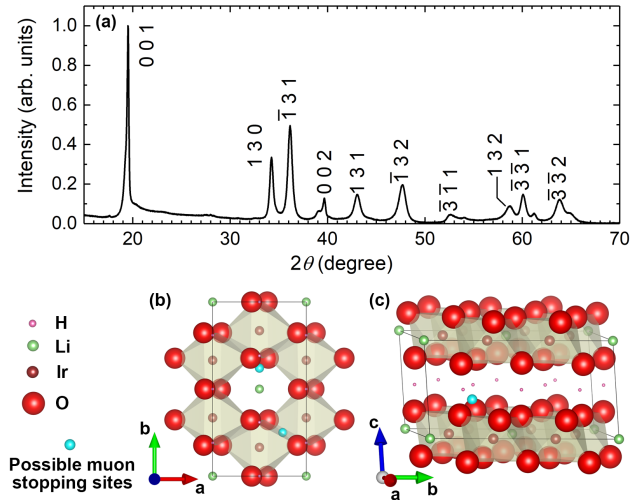


FIG. 1. Sample characterizations and its crystal structure. (a) Powder XRD pattern of $\text{H}_3\text{LiIr}_2\text{O}_6$ at room temperature. (b) and (c) Crystal structures viewed from c -axis and a -axis, respectively. Pink spheres: H^+ ions. Green spheres: Li^+ ions. Brown spheres: Ir^{3+} ions. Red spheres: O^{2-} ions. Cyan points: three possible muon stopping sites.

reveal the disorder-induced exotic excitations characteristic of the Kitaev QSL.

Experimental setup and sample characterizations. – XRD measurements were conducted on Rigaku Smartlab 9KW using $\text{Cu K}\alpha$ radiation at room temperature. Magnetic susceptibility measurements were carried out on a Quantum Design SQUID magnetometer. The specific heat was measured for $0.1 \text{ K} \leq T \leq 50 \text{ K}$ on a Quantum Design Physical Properties Measurement System semi-adiabatic calorimeter using a heat-pulse technique. μSR experiments were carried out down to 80 mK and longitudinal external magnetic field up to 0.3 T on μSR spectrometer at ISIS Neutron and Muon Facility, Rutherford Appleton Laboratory Chilton, UK. Spin-polarized positive muons were implanted into 1 gram of polycrystalline sample mounted on a silver sample holder covering a circular area of 1 inch in diameter.

Polycrystalline sample of $\text{H}_3\text{LiIr}_2\text{O}_6$ was prepared by the cation exchange reaction [22, 23]. The starting materials Li_2CO_3 and IrO_2 powder were mixed thoroughly in the ratio of 1.05 : 1, and placed in an alumina crucible with a lid and annealed at 840°C for one day to obtain the precursor $\alpha\text{-Li}_2\text{IrO}_3$ powder. For the cation exchange, $\alpha\text{-Li}_2\text{IrO}_3$ powder was added into a Teflon-lined steel autoclave with 4 mol/L H_2SO_4 aqueous solution. The mixture was heated in the sealed vessel at 120°C for one hour. Polycrystalline $\text{H}_3\text{LiIr}_2\text{O}_6$ was obtained by washing with distilled water and dried at 80°C .

The powder X-ray diffraction (PXRD) pattern of $\text{H}_3\text{LiIr}_2\text{O}_6$ in Fig. 1 shows that several diffraction pattern peaks are broaden and even disappear, suggesting the

heavily stacking faulted crystal structure. Our PXRD pattern agrees with the previous results [22, 23], and the stable phase $\text{H}_3\text{LiIr}_2\text{O}_6$ was confirmed from the synthetics evolution process ($\alpha\text{-Li}_2\text{IrO}_3 \rightarrow \text{H}_3\text{LiIr}_2\text{O}_6 \rightarrow \text{H}_5\text{LiIr}_2\text{O}_6$) [24].

There are several forms of non-magnetic disorders in $\text{H}_3\text{LiIr}_2\text{O}_6$. The first-generation iridate $\alpha\text{-Li}_2\text{IrO}_3$ already manifests stacking faults along the c -axis [20, 35]. The chemical modification further increases the stacking faults in the second-generation iridate $\text{H}_3\text{LiIr}_2\text{O}_6$ [22–24, 36], indicated by the broad and weak PXRD peaks in Fig. 1. Compared with $\alpha\text{-Li}_2\text{IrO}_3$, previous Raman studies also revealed an unusual phonon broadening in $\text{H}_3\text{LiIr}_2\text{O}_6$ [20, 24], implying the random positions of the substituted H^+ , probably causing the bond disorders [26, 33]. During the soft-chemical-ion exchange of Li^+ and H^+ , more hydrogen atoms could intercalate into the interlayers of $[\text{LiIr}_2\text{O}_6]$ layers in $\text{H}_3\text{LiIr}_2\text{O}_6$, and lower the iridium ion oxidation state from Ir^{4+} into Ir^{3+} , signaled by the XPS measurements [24]. Ir^{3+} has a $3d^6$ electronic configuration and fully occupied t_{2g} orbitals, serving as the non-magnetic impurity in $\text{H}_3\text{LiIr}_2\text{O}_6$. All the non-magnetic disorders can induce abundant low-energy DOS [33, 34, 36].

Thermodynamic properties and low-energy DOS. – We performed thermodynamic magnetization and heat capacity measurements of our powder samples $\text{H}_3\text{LiIr}_2\text{O}_6$. The results are overall consistent with the previous report [23] and also have the discrepancy in several details, probably due to different

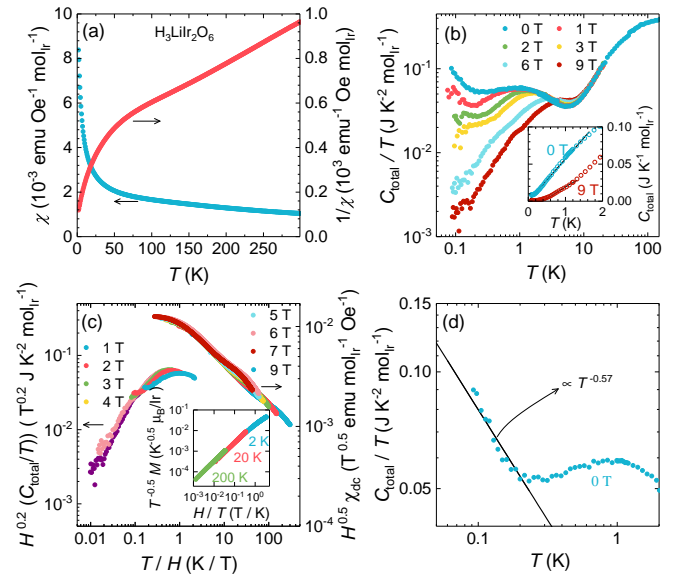


FIG. 2. (a) Temperature dependence of magnetic susceptibility and its reciprocal of $\text{H}_3\text{LiIr}_2\text{O}_6$ measured at $\mu_0 H = 1 \text{ T}$. (b) Total specific heat C_{total} divided by T as a function of T under the field of 0 T, 1 T, 2 T, 3 T, 6 T and 9 T. Inset: C_{total} versus T at 0 T and 9 T. The solid curves are $C_{\text{total}} \sim \gamma T$ for 0 T and $C_{\text{total}} \sim e^{-\frac{\Delta}{T}}$ for 9 T. (c) Scaling plot of $H^{0.2} C_{\text{total}}/T$ vs T/H , $H^{0.5} \chi_{\text{dc}}$ with T/H , and $T^{-0.5} M(H)$ vs H/T . (d) Specific heat C_{total} divided by T as a function of T . Since the lattice contribution C_{lattice} of specific heat is negligible below 2 K, $C_{\text{total}}/T \simeq C_M/T$. Black line: $C_M/T = 0.02T^{-0.57}$.

concentrations of disorders. Fig. 2 (a) shows the temperature dependence of magnetic susceptibility $\chi(T)$ of $\text{H}_3\text{LiIr}_2\text{O}_6$ measured under an external field of $\mu_0 H = 1$ T. According to the Curie-Weiss behavior at high temperatures, $\text{H}_3\text{LiIr}_2\text{O}_6$ has overall antiferromagnetic interactions with the energy scale of the order of 100 K, but no trace of magnetic ordering is observed in $\chi(T)$ down to 2 K, in sharp contrast to other Kitaev candidates [16, 37–39]. The absence of magnetic ordering is further confirmed by the heat capacity measurements down to 0.1 K as shown in Fig. 2 (b), which shows the temperature dependence of C_{total}/T under several applied magnetic fields. At zero magnetic field, a low-temperature plateau followed by a low-temperature divergence in the specific heat coefficient C/T is obvious. The altitude of the plateau is about $58 \text{ mJ K}^2 \text{ mol-Ir}^{-1}$ and is gradually suppressed by the magnetic fields. The specific heat data taken under $\mu_0 H = 9$ T is well fitted by $C \sim e^{-\frac{\Delta}{T}}$ with $\Delta = 1.6$ K. The low-temperature plateau of the specific heat coefficient C/T in $\text{H}_3\text{LiIr}_2\text{O}_6$ is likely related to the disorder-induced states which are suppressed in magnetic fields [23, 33, 34].

At relatively high fields (larger than 1 T), we can plot $H^{1-\alpha_c} C/T$ against the single dimensionless variable T/H , and the data overlap over 2 orders of magnitude with $\alpha_c = 0.8$ as shown in Fig. 2 (c). We notice that the low-temperature upturn in the specific heat data at $\mu_0 H = 1$ T deviates from the data collapse, consistent with the theoretical simulations for disorder effect in the Kitaev QSL where the scaling behavior only appears at high fields [34]. The magnetization results also have the scaling behavior in $H^{\alpha_m} \chi$, and $T^{\alpha_m-1} M$ against the single dimensionless variable T/H with $\alpha_m = 0.5$. The scaling behaviors of heat capacity and magnetization at relatively high fields are also reported in other disordered Kitaev materials [40–42].

The specific heat coefficient has a divergence of $C/T \sim T^{-0.57}$ below 0.2 K at zero magnetic fields was observed in our polycrystalline sample of $\text{H}_3\text{LiIr}_2\text{O}_6$. We attribute this to the intrinsic behavior of magnetic specific heat of $\text{H}_3\text{LiIr}_2\text{O}_6$ since lattice contribution to the specific heat is negligible below $T = 2$ K. The low-temperature divergence is suppressed by the applied magnetic field, at odds with nuclear Schottky contribution that usually survives under magnetic fields of a few Tesla. The C/T divergence is consistent with a power-law low energy DOS of the theoretical form $N(E) \sim E^{-0.5}$ [34], deviating from the power characteristic of the pure Dirac dispersion of Majorana fermions in the pure Kitaev QSL. Theoretically, a finite density of random vacancies in the Kitaev model gives rise to a pileup of low-energy Majorana eigenmodes accounting for the power-law upturn in the specific heat measurements [23, 33, 34]. The power-law upturn at low magnetic fields doesn't fit the heat capacity scaling in Fig. 2 (c) for the relatively-high-field heat capacity [34].

Spin dynamics in μSR . – The power-law divergence $C/T \sim T^{-0.57}$ in $\text{H}_3\text{LiIr}_2\text{O}_6$ persists down to 0.1 K, indicating a low energy scale for the power-law DOS. The power-law DOS should also give rise to a power-law scaling in the spin dynamics that can be tested in the muon spin relaxation study,

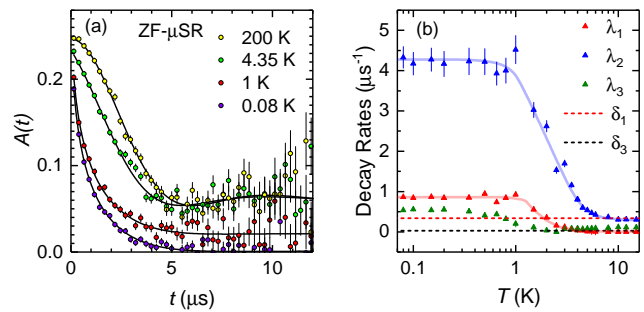


FIG. 3. (a) ZF- μSR spectra of $\text{H}_3\text{LiIr}_2\text{O}_6$ at selected temperatures. Colored lines are the fits to raw data using Eq. (2). (b) Temperature dependence of muon spin relaxation rates.

which is the main purpose of the present work.

Implanted muons are sensitive to local magnetic fields induced by the neighboring Ir^{4+} spins. Fig. 3 (a) shows the representative time evolution of the decay position count rate asymmetry $A(t)$, proportional to the positive muon spin polarization $P(t)$, in $\text{H}_3\text{LiIr}_2\text{O}_6$, from $T = 200$ K down to lowest measured temperature 0.08 K at zero field. A constant background signal ($A = 0.015$), which originates from muons that miss the sample and stop in the silver sample holder, has been subtracted from the data. As decreasing temperatures, the initial shape of ZF- μSR spectra changes from the Gaussian to the Lorentzian like, suggesting strong dynamic spin fluctuations at low temperatures. Down to the lowest temperature, no evidence of magnetic order was found, since neither oscillations nor a drastic drop in the initial asymmetry appears.

At zero magnetic field, a Gaussian distribution of randomly oriented static (or quasi-static) local fields gives rise to the decay of muon polarization $P(t)$ in the Gaussian Kubo-Toyabe form [43]

$$G_{\text{KT}}(\delta, t) = \frac{1}{3} + \frac{2}{3}(1 - \delta^2 t^2)e^{-\frac{1}{2}\delta^2 t^2}, \quad (1)$$

with the distribution width δ/γ_μ for the quasi-static local fields, where $\gamma_\mu = 2\pi \times 135.53 \text{ MHz/T}$ is the μ^+ gyromagnetic ratio. If local fields associated with the magnetic moments fluctuates strongly, $P(t)$ is usually well approximated by a Lorentzian exponential function characterized by the relaxation rate λ , $P(t) \sim \exp(-\lambda t)$.

The asymmetry of ZF- μSR spectra in $\text{H}_3\text{LiIr}_2\text{O}_6$ cannot be described in terms of only the Kubo-Toyabe type, or the simple exponential function. They are best fitted by several components by the following function

$$A(t) = A_1 \exp(-\lambda_1 t) G_{\text{KT}}(\delta_1, t) + A_2 \exp(-\lambda_2 t) + A_3 \exp(-\lambda_3 t) G_{\text{KT}}(\delta_3, t). \quad (2)$$

$A_{1,2,3}$ in Eq. (2) denotes the initial asymmetry for three different depolarization components. The total initial asymmetry ($A_1 + A_2 + A_3$) decreases slightly on cooling along with the increasing decay rates. This tiny loss of initial asymmetry is

attributed to the time resolution of pulse beamline with pulse width of 80 ns [44, 45]. The ratio of A_1 to A_2 was fixed at the value of 2, determined from LF- μ SR experiments, in which the relaxation is purely dynamic and its analysis is simplified described later. $A_{1,2,3}$ is found to be temperature independent with $A_1 = 0.113$, $A_2 = 0.056$, and $A_3 = 0.069$.

Figure 3 (b) shows the ZF temperature dependence of muon spin relaxation rates $\lambda_{1,2,3}$ and $\delta_{1,2}$ in $\text{H}_3\text{LiIr}_2\text{O}_6$. $\delta_{1,2}$ is roughly temperature independent and was fixed at an average values. We attribute this Gaussina field distribution $\delta_{1,2}$ to nuclear dipolar fields. A drastic increase of $\lambda_{1,2,3}$ below $T = 3$ K is observed, accompanied by the growing magnetic contribution to the specific heat. So the spin dynamics is related to the disorder-induced DOS in the Kitaev QSL. The increase of $\lambda_{1,2,3}$ saturates below 1K, and remains almost constant down to the lowest measured temperature. The low temperature plateau of λ excludes the spin glass state and indicates the persistent spin dynamics and large density of states at low energies.

To further measure the spin dynamics, we performed LF- μ SR measurements with an external field in the direction of the initial muon spin polarization. The longitudinal-field $\mu_0 H = 100$ mT was chosen to be much larger than the static field estimated from the ZF- μ SR $\delta/\gamma_\mu \sim 0.4$ mT, so that the static or quasi-static field is completely decoupled [43] and one observes only the dynamic relaxation. Representative LF- μ SR spectra $P_\mu(t)$ for different temperatures are shown in Fig. 4 (b). In order to compare with ZF- μ SR, a constant background signal of 0.015 is also subtracted in Fig. 4 (b). The LF spectra are well described by the functional form

$$A(t) = A_1 e^{-\lambda_1 t} + A_2 e^{-\lambda_2 t} + A_3, \quad (3)$$

where $A_{1,2,3}$ has the same meaning of that in Eq. (2), but with slightly smaller values. λ_3 in Eq. (2) is negligible under magnetic field $\mu_0 H = 0.1$ T, therefore it is set to be zero in Eq. (3).

Temperature dependence of LF relaxation rates λ_1 and λ_2 has the same character that they gradually increase on cooling and saturate at $0.16 \mu\text{s}^{-1}$ and $1.3 \mu\text{s}^{-1}$ respectively at low temperatures as shown in Fig. 4 (b). The low temperature

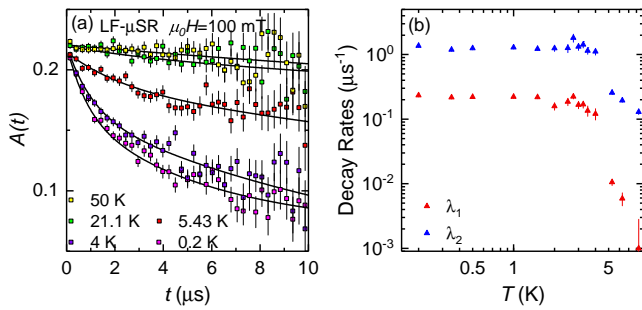


FIG. 4. (a) LF- μ SR spectra of $\text{H}_3\text{LiIr}_2\text{O}_6$ at selected temperatures. Colored lines are fits to the raw data using Eq. (3). (b) Temperature dependence of LF muon spin relaxation rates.

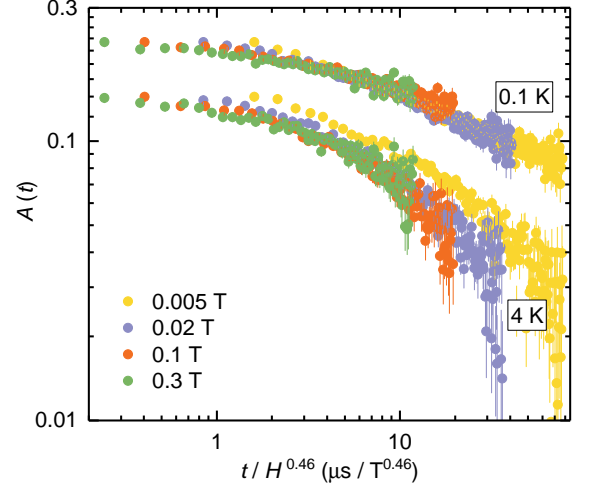


FIG. 5. Time-field scaling of μ SR spectra $A(t) \sim t/B^{0.46}$ at 0.1 K and 4 K in $\text{H}_3\text{LiIr}_2\text{O}_6$.

plateaus of both λ_1 and λ_2 indicate that the spins in system are highly frustrated and persistent spin dynamics take place even under $\mu_0 H = 100$ mT magnetic field applied.

The temperature independent $A_{1,2,3}$ and the similar temperature dependence of $\lambda_{1,2,3}$ for both ZF and LF experiments suggests that the three components in Eq. (2) or Eq. (3) are due to distinct μ^+ interstitial stopping sites. In addition, the ratio of λ_2/λ_1 is 5.0(5) for ZF measurements, and 5.6(3) for LF measurements at low temperatures. Within error the same ratio suggests that the two exponential relaxations are due to differences in coupling fields rather than inhomogeneity in the spin dynamics. This is expected when the fluctuation rates at the different sites are the same and the correlation length for the fluctuations is short [46, 47], and therefore is additional evidence for the multi-site scenario. The possible muon stopping sites are suggested as marked by cyan points in Fig. 1 (b) and (c). One is between the Ir^{4+} ion and the nearest neighbor Li^+ ion, and the other is between two nearest neighbor Ir^{4+} ions, since the ratio of quantity between Ir-Li bonds and Ir-Ir bonds is 2:1 in $\text{H}_3\text{LiIr}_2\text{O}_6$, and the absence of KT relaxation rate for the second stie is due to the nearby Ir atoms, which do not have nuclear moments. The third possible stopping site is between Ir layers, and close to the random H^+ ions, since muon experience relatively weaker spin dynamics and nuclear moments.

The increasing low-temperature spin dynamics in ZF- and LF- μ SR is accompanied by the growing magnetic contribution to the specific heat, and likely has the origin of the disordered-induced low-energy DOS in $\text{H}_3\text{LiIr}_2\text{O}_6$. The DOS has the critical form of $N(E) \sim E^{-1/2}$, which may cause the power-law scaling of the spin dynamics measured in μ SR. LF- μ SR measurements in applied LF between 1 mT and 300 mT at $T = 0.1$ K and 4 K were carried out to study the low-energy

spin dynamics in $\text{H}_3\text{LiIr}_2\text{O}_6$. The field dependence of λ_1 and λ_2 can be described as $\lambda_{1,2}(H) = H^{-n_{1,2}} + c_{1,2}$, where $c_{1,2}$ are constants and $n_1 \approx n_2 = 0.46$. The power-law behaviors of $\lambda(H)$ indicates the time-field scaling of LF- μSR spectra [48, 49]. Therefore we have plotted the relaxation function against the scaling variable (t/H^α with $\alpha = 0.46$), as shown in Fig. 5. The observation of the time-field scaling can be interpreted as a signature of power-law low-energy spin dynamics, $q(t) = \langle S_i(t) \cdot S_i(0) \rangle \sim t^{\alpha-1} \exp(-\lambda t)$ [48, 49].

We argue that the power-law low-energy spin dynamics is related to disorder-induced low-energy DOS in the Kitaev QSL. For the pure Kitaev model, the spin operator is written in terms of Majorana fermions $S_i^a = \frac{i}{2} b_i^a c_i$ where b_i^a is related to the flux and c_i represents the low-energy Majorana excitations. The spin-spin autocorrelation function is $q(t) = \langle S_i(t) \cdot S_i(0) \rangle \sim \langle c_i(t) c_i(0) \rangle \exp(-\lambda t)$ where we assume the time evolution is dominated by the low-energy excitations c_i and the time revolution of b_i^a gives rise to $\exp(-\lambda t)$. Thus $q(t)$ is related to the Green function of the low-energy Majorana excitation c_i , and can be taken as the Fourier transformation of the DOS

$$\begin{aligned} q(t) &\sim \exp(-\lambda t) \int N(E) \exp(-Et) dE \\ &= t^{\alpha-1} \exp(-\lambda t) \int (Et)^{-\alpha} \exp(-Et) d(Et) \\ &\sim t^{\alpha-1} \exp(-\lambda t). \end{aligned} \quad (4)$$

Therefore, the time-field scaling of LF- μSR $A(t) \sim t/B^\alpha$ ($\alpha = 0.46$) in Fig. 5 implies the low-energy DOS in the form $N(E) \sim E^{-\alpha}$ with the theoretical value of $\alpha = 0.5$, consistent with the heat capacity low-temperature upturn $C/T \sim T^{-\alpha}$ ($\alpha = 0.57$) at low temperatures in Fig. 2(d).

Conclusions.— $\text{H}_3\text{LiIr}_2\text{O}_6$ has various disorder forms of stacking faults, randomness of H^+ positions and non-magnetic impurities Ir^{3+} with lower oxidation state due to excess hydrogen. The disorders could suppress long-range magnetic order and also induce low-energy density of states in the Kitaev quantum spin liquid materials. Our thermodynamic and μSR measurements reveal no sign of static magnetic ordering, establishing a quantum spin-liquid ground state in $\text{H}_3\text{LiIr}_2\text{O}_6$. Furthermore, the low-temperature power-law specific heat coefficient $C/T \sim T^{-0.57}$ and time-field scaling of longitudinal-field μSR $A(t) \sim t/B^{0.46}$ indicate the finite density of state in the form $N(E) \sim E^{-0.5}$, in a good agreement with the disorder-induced states in the Kitaev spin liquid.

Acknowledgments – We are grateful to the ISIS cryogenics Group for their valuable help during the μSR experiments (10.5286/ISIS.E.RB1910121). The work at Fudan University is supported by the National Natural Science Foundation of China under Grant No. 12034004 and N0. 12174065, and the Shanghai Municipal Science and Technology (Major Project Grant No. 2019SHZDZX01 and No. 20ZR1405300). The work at SUSTech was supported by the Science, Technology and Innovation Commission of Shenzhen Municipality (No. ZDSYS20170303165926217) and the program

for Guangdong Introducing Innovative and Entrepreneurial Teams (No. 2017ZT07C062).

* These two authors contribute to this work equally.

† meijw@sustech.edu.cn

‡ leishu@fudan.edu.cn

- [1] P. W. Anderson, Resonating valence bonds: A new kind of insulator?, *Mater. Res. Bull.* **8**, 153 (1973).
- [2] P. W. Anderson, The Resonating Valence Bond State in La_2CuO_4 and Superconductivity, *Science* **235**, 1196 (1987), <https://www.science.org/doi/pdf/10.1126/science.235.4793.1196>.
- [3] A. Kitaev, Anyons in an exactly solved model and beyond, *Annals of Physics* **321**, 2 (2006).
- [4] X.-G. Wen and M. Fisher, Quantum field theory of many-body systems: From the origin of sound to an origin of light and electrons, *Physics Today* **58**, 52 (2005).
- [5] A. Kitaev and J. Preskill, Topological entanglement entropy, *Phys. Rev. Lett.* **96**, 110404 (2006).
- [6] M. Levin and X.-G. Wen, Detecting topological order in a ground state wave function, *Phys. Rev. Lett.* **96**, 110405 (2006).
- [7] X.-G. Wen, Colloquium: Zoo of quantum-topological phases of matter, *Rev. Mod. Phys.* **89**, 041004 (2017).
- [8] X.-G. Wen, Choreographed entanglement dances: Topological states of quantum matter, *Science* **363**, eaal3099 (2019).
- [9] A. Y. Kitaev, Fault-tolerant quantum computation by anyons, *Annals of Physics* **303**, 2 (2003).
- [10] G. Jackeli and G. Khaliullin, Mott insulators in the strong spin-orbit coupling limit: From heisenberg to a quantum compass and kitaev models, *Phys. Rev. Lett.* **102**, 017205 (2009).
- [11] J. c. v. Chaloupka, G. Jackeli, and G. Khaliullin, Kitaev-Heisenberg Model on a Honeycomb Lattice: Possible Exotic Phases in Iridium Oxides A_2IrO_3 , *Phys. Rev. Lett.* **105**, 027204 (2010).
- [12] H. Takagi, T. Takayama, G. Jackeli, G. Khaliullin, and S. E. Nagler, Concept and realization of kitaev quantum spin liquids, *Nat. Rev. Phys.* **1**, 264 (2019).
- [13] S. K. Choi, R. Coldea, A. N. Kolmogorov, T. Lancaster, I. I. Mazin, S. J. Blundell, P. G. Radaelli, Y. Singh, P. Gegenwart, K. R. Choi, S. W. Cheong, P. J. Baker, C. Stock, and J. Taylor, Spin Waves and Revised Crystal Structure of Honeycomb Iridate Na_2IrO_3 , *Phys. Rev. Lett.* **108**, 127204 (2012).
- [14] Y. Singh, S. Manni, J. Reuther, T. Berlijn, R. Thomale, W. Ku, S. Trebst, and P. Gegenwart, Relevance of the Heisenberg-Kitaev Model for the Honeycomb Lattice Iridates A_2IrO_3 , *Phys. Rev. Lett.* **108**, 127203 (2012).
- [15] K. W. Plumb, J. P. Clancy, L. J. Sandilands, V. V. Shankar, Y. F. Hu, K. S. Burch, H.-Y. Kee, and Y.-J. Kim, $\alpha - \text{RuCl}_3$: A spin-orbit assisted Mott insulator on a honeycomb lattice, *Phys. Rev. B* **90**, 041112 (2014).
- [16] S. Hwan Chun, J.-W. Kim, J. Kim, H. Zheng, C. C. Stoumpos, C. D. Malliakas, J. F. Mitchell, K. Mehlawat, Y. Singh, Y. Choi, T. Gog, A. Al-Zein, M. M. Sala, M. Krisch, J. Chaloupka, G. Jackeli, G. Khaliullin, and B. J. Kim, Direct evidence for dominant bond-directional interactions in a honeycomb lattice iridate Na_2IrO_3 , *Nat. Phys.* **11**, 462 (2015).
- [17] R. D. Johnson, S. C. Williams, A. A. Haghighirad, J. Singleton, V. Zapf, P. Manuel, I. I. Mazin, Y. Li, H. O. Jeschke, R. Valentí, and R. Coldea, Monoclinic crystal structure of $\alpha - \text{RuCl}_3$ and the zigzag antiferromagnetic ground state, *Phys. Rev. B* **92**, 235119 (2015).

- [18] S. C. Williams, R. D. Johnson, F. Freund, S. Choi, A. Jesche, I. Kimchi, S. Manni, A. Bombardi, P. Manuel, P. Gegenwart, and R. Coldea, Incommensurate counterrotating magnetic order stabilized by Kitaev interactions in the layered honeycomb α -Li₂IrO₃, *Phys. Rev. B* **93**, 195158 (2016).
- [19] A. Glamazda, P. Lemmens, S. H. Do, Y. S. Choi, and K. Y. Choi, Raman spectroscopic signature of fractionalized excitations in the harmonic-honeycomb iridates β - and γ -Li₂IrO₃, *Nat. Commun.* **7**, 12286 (2016).
- [20] G. Li, L.-L. Huang, X. Chen, C. Liu, S. Pei, X. Wang, S. Wang, Y. Zhao, D. Yu, L. Wang, F. Ye, J.-W. Mei, and M. Huang, Probing the continuum scattering and magnetic collapse in single-crystalline α -Li₂IrO₃ by Raman spectroscopy, *Phys. Rev. B* **101**, 174436 (2020).
- [21] A. Banerjee, J. Yan, J. Knolle, C. A. Bridges, M. B. Stone, M. D. Lumsden, D. G. Mandrus, D. A. Tennant, R. Moessner, and S. E. Nagler, Neutron scattering in the proximate quantum spin liquid α -RuCl₃, *Science* **356**, 1055 (2017), <https://www.science.org/doi/pdf/10.1126/science.aah6015>.
- [22] S. Bette, T. Takayama, K. Kitagawa, R. Takano, H. Takagi, and R. E. Dinnebier, Solution of the heavily stacking faulted crystal structure of the honeycomb iridate H₃LiIr₂O₆, *Dalton Trans.* **46**, 15216 (2017).
- [23] K. Kitagawa, T. Takayama, Y. Matsumoto, A. Kato, R. Takano, Y. Kishimoto, S. Bette, R. Dinnebier, G. Jackeli, and H. Takagi, A spin-orbital-entangled quantum liquid on a honeycomb lattice, *Nature* **554**, 341 (2018).
- [24] S. Pei, L.-L. Huang, G. Li, X. Chen, B. Xi, X. Wang, Y. Shi, D. Yu, C. Liu, L. Wang, F. Ye, M. Huang, and J.-W. Mei, Magnetic Raman continuum in single-crystalline H₃LiIr₂O₆, *Phys. Rev. B* **101**, 201101 (2020).
- [25] J. Knolle, G.-W. Chern, D. L. Kovrizhin, R. Moessner, and N. B. Perkins, Raman Scattering Signatures of Kitaev Spin Liquids in A₂IrO₃ Iridates with A=Na or Li, *Phys. Rev. Lett.* **113**, 187201 (2014).
- [26] Y. Li, S. M. Winter, and R. Valentí, Role of Hydrogen in the Spin-Orbital-Entangled Quantum Liquid Candidate H₃LiIr₂O₆, *Phys. Rev. Lett.* **121**, 247202 (2018).
- [27] A. Andreanov, J. T. Chalker, T. E. Saunders, and D. Sherrington, Spin-glass transition in geometrically frustrated antiferromagnets with weak disorder, *Phys. Rev. B* **81**, 014406 (2010).
- [28] R. R. P. Singh, Valence bond glass phase in dilute kagome antiferromagnets, *Phys. Rev. Lett.* **104**, 177203 (2010).
- [29] L. Savary and L. Balents, Disorder-induced quantum spin liquid in spin ice pyrochlores, *Phys. Rev. Lett.* **118**, 087203 (2017).
- [30] A. Sen and R. Moessner, Topological spin glass in diluted spin ice, *Phys. Rev. Lett.* **114**, 247207 (2015).
- [31] I. Kimchi, A. Nahum, and T. Senthil, Valence Bonds in Random Quantum Magnets: Theory and Application to YbMgGaO₄, *Phys. Rev. X* **8**, 031028 (2018).
- [32] I. Kimchi, J. P. Shekelton, T. M. McQueen, and P. A. Lee, Scaling and data collapse from local moments in frustrated disordered quantum spin systems, *Nat. Commun.* **9**, 4367 (2018).
- [33] J. Knolle, R. Moessner, and N. B. Perkins, Bond-Disordered Spin Liquid and the Honeycomb Iridate H₃LiIr₂O₆: Abundant Low-Energy Density of States from Random Majorana Hopping, *Phys. Rev. Lett.* **122**, 047202 (2019).
- [34] W.-H. Kao, J. Knolle, G. B. Halász, R. Moessner, and N. B. Perkins, Vacancy-induced low-energy density of states in the kitaev spin liquid, *Phys. Rev. X* **11**, 011034 (2021).
- [35] F. Freund, S. C. Williams, R. D. Johnson, R. Coldea, P. Gegenwart, and A. Jesche, Single crystal growth from separated educts and its application to lithium transition-metal oxides, *Sci. Rep.* **6**, 35362 (2016).
- [36] K. Slagle, W. Choi, L. E. Chern, and Y. B. Kim, Theory of a quantum spin liquid in the hydrogen-intercalated honeycomb iridate H₃LiIr₂O₆, *Phys. Rev. B* **97**, 115159 (2018).
- [37] M. Abramchuk, C. Ozsoy-Keskinbora, J. W. Krizan, K. R. Metz, D. C. Bell, and F. Tafti, Cu₂IrO₃: A New Magnetically Frustrated Honeycomb Iridate, *J. Am. Chem. Soc.* **139**, 15371 (2017).
- [38] S. Choi, S. Manni, J. Singleton, C. V. Topping, T. Lancaster, S. J. Blundell, D. T. Adroja, V. Zapf, P. Gegenwart, and R. Coldea, Spin dynamics and field-induced magnetic phase transition in the honeycomb Kitaev magnet α -Li₂IrO₃, *Phys. Rev. B* **99**, 054426 (2019).
- [39] K. Ran, J. Wang, W. Wang, Z. Y. Dong, X. Ren, S. Bao, S. Li, Z. Ma, Y. Gan, Y. Zhang, J. T. Park, G. Deng, S. Danilkin, S. L. Yu, J. X. Li, and J. Wen, Spin-Wave Excitations Evidencing the Kitaev Interaction in Single Crystalline α -RuCl₃, *Phys. Rev. Lett.* **118**, 107203 (2017).
- [40] Y. S. Choi, C. H. Lee, S. Lee, S. Yoon, W.-J. Lee, J. Park, A. Ali, Y. Singh, J.-C. Orain, G. Kim, J.-S. Rhyee, W.-T. Chen, F. Chou, and K.-Y. Choi, Exotic Low-Energy Excitations Emergent in the Random Kitaev Magnet Cu₂IrO₃, *Phys. Rev. Lett.* **122**, 167202 (2019).
- [41] F. Bahrami, W. Lafargue-Dit-Hauret, O. I. Lebedev, R. Movshovich, H.-Y. Yang, D. Broido, X. Rocquefelte, and F. Tafti, Thermodynamic Evidence of Proximity to a Kitaev Spin Liquid in Ag₃LiIr₂O₆, *Phys. Rev. Lett.* **123**, 237203 (2019).
- [42] S.-H. Do, C. H. Lee, T. Kihara, Y. S. Choi, S. Yoon, K. Kim, H. Cheong, W.-T. Chen, F. Chou, H. Nojiri, and K.-Y. Choi, Randomly Hopping Majorana Fermions in the Diluted Kitaev System α -Ru_{0.8}Ir_{0.2}Cl₃, *Phys. Rev. Lett.* **124**, 047204 (2020).
- [43] R. S. Hayano, Y. J. Uemura, J. Imazato, N. Nishida, T. Yamazaki, and R. Kubo, Zero- and low-field spin relaxation studied by positive muons, *Phys. Rev. B* **20**, 850 (1979).
- [44] S. R. Giblin, S. P. Cottrell, P. J. C. King, S. Tomlinson, S. J. S. Jago, L. J. Randall, M. J. Roberts, J. Norris, S. Howarth, Q. B. Mutamba, N. J. Rhodes, and F. A. Akeroyd, Optimising a muon spectrometer for measurements at the isis pulsed muon source, *Nucl. Instruments Methods Phys. Res. Sect. A* **751**, 70 (2014).
- [45] A. D. Hillier, S. P. Cottrell, P. J. C. King, G. H. Eaton, and M. A. Clarke-Gayther, High frequency measurements at a pulsed muon source: beating the pulse width!, *Physica B: Condensed Matter* **326**, 275 (2003).
- [46] X. F. Miao, L. Caron, J. Cedervall, P. C. M. Gubbens, P. Dalmas de Réotier, A. Yaouanc, F. Qian, A. R. Wildes, H. Luetkens, A. Amato, N. H. van Dijk, and E. Brück, Short-range magnetic correlations and spin dynamics in the paramagnetic regime of (Mn, Fe)₂(P, Si), *Phys. Rev. B* **94**, 014426 (2016).
- [47] Z. Ding, Z. Zhu, J. Zhang, C. Tan, Y. Yang, D. E. MacLaughlin, and L. Shu, Persistent spin dynamics and absence of spin freezing in the h - t phase diagram of the two-dimensional triangular antiferromagnet ybmga₄, *Phys. Rev. B* **102**, 014428 (2020).
- [48] A. Keren, P. Mendels, I. A. Campbell, and J. Lord, Probing the Spin-Spin Dynamical Autocorrelation Function in a Spin Glass above T_f via Muon Spin Relaxation, *Phys. Rev. Lett.* **77**, 1386 (1996).
- [49] A. Keren, Muons as probes of dynamical spin fluctuations: some new aspects, *Journal of Physics: Condensed Matter* **16**, S4603 (2004).